Available online at www.sciencedirect.com
ScienceDirect
International Journal of Thermal Sciences 46 (2007) 1297–1303
International Journal of Thermal Sciences
www.elsevier.com/locate/ijts

Heat transfer enhancement in circular tubes using helical swirl generator insert at the entrance

H. Gül [a], D. Evin [b,*]

[a] *Fırat University, Vocational High School, 23119, Elazığ, Turkey*
[b] *Fırat University, Mechanical Engineering Faculty, 23119 Elazığ, Turkey*

Received 31 May 2006; received in revised form 21 December 2006; accepted 22 December 2006
Available online 15 February 2007

Abstract

This paper presents an experimental study of heat transfer and friction characteristics in decaying turbulent swirl flow generated by a short helical tape placed at the entrance of the test section. In the experiments, total mass flux was varied from 160 kg m^{-2} s^{-1} to 1628 kg m^{-2} s^{-1} and the momentum ratio (M_h/M_T) was varied from 0 to 8.6. The experiments were conducted for water flow rates in the range of $5000 \leqslant Re \leqslant 30\,000$. Three different helical tapes with helical angels of 30°, 45° and 60° were used. Experimental results confirm that, the use of a helical tape inserted to the tube leads to a higher heat transfer rate than the non-swirling flow. The local heat transfer coefficients were found to be increasing to very high values along the downstream of the helical tape, and then decreasing with the distance (x/L). The augmentation of heat transfer was found to be the function of the momentum ratio, M_h/M_T and Reynolds number. No pronounced effect of the number of the helical channels (N_h), and helical angle (α) on heat transfer was observed. It is found that using the helical tape can help to increase the heat transfer rate up to 20% depending on M_h/M_T and Re at constant pumping power. Enhancement efficiency increases with increasing momentum ratio and decreases with increasing Reynolds number.

Keywords: Heat transfer enhancement; Circular tubes; Swirl flow; Helical tape

1. Introduction

Swirl flow has been used in a wide range of applications form various engineering areas such as chemical and mechanical mixing and separation devices, combustion chambers, turbo machinery to pollution control devices. It is commonly known that the swirl flow enhances the heat transfer mainly due to the increased velocity in the swirl tube and the circulation of the fluid by centrifugal convection because the low density of the warmer fluid at the pipe wall is displaced into the cooler stream in the central region by centripetal force.

There have been numerous attempts to reduce the size and cost of heat exchangers. For this purpose, first a study of the heat transfer coefficient and friction factor for the system under investigation must be carried out. A lot of techniques have been proposed by many investigators for the improvement of heat transfer. Smithberg and Landis [1] reported friction and forced convection heat transfer characteristics in tubes fitted with twisted tape swirl generators, and presented a correlation for predicting Nusselt number and friction factor. Date and Singham [2], and Date [3] reported the prediction of fully developed flow in a tube containing a twisted tape. Hong and Bergles [4] correlated heat transfer and pressure drop date for twisted tape inserts for uniform wall temperature conditions using water as working fluids in laminar flow. Eiamsa-ard, and Promvonge [5] reported the enhancement of the heat transfer in a tube with regularly spaced and full-length helical tape swirl generators, and concluded that the full-length helical tape with rod provide the highest heat transfer rate about 10% better than without rod.

To increase heat transfer coefficient, rotating or secondary flow on axial forced flow, such as inlet vortex generators, twisted-tapes and axial core inserts are being used. Some of these methods generate swirl flow continuously along the entire

* Corresponding author. Tel.: +90 424 2370000/5334; fax: +90 424 2415526.
E-mail addresses: hgul@firat.edu.tr (H. Gül), devin@firat.edu.tr (D. Evin).

1290-0729/$ – see front matter
doi:10.1016/j.ijthermalsci.2006.12.010

Nomenclature

A	heat transfer area of the pipe	m^2
A_h	cross-sectional flow area of the helical channel	m^2
b	mean channel width	m
C_p	specific heat	$kJ\,kg^{-1}\,K^{-1}$
D_0	test tube outer diameter	m
D_i	test tube inner diameter	m
D_h	hydraulic diameter of the channel	m
d_1	inner diameter of the helical tape	m
d_2	outer diameter of the helical tape	m
f	friction factor	
H	helical channel depth	m
h	heat transfer coefficient	$W\,m^{-2}\,K^{-1}$
k	thermal conductivity	$W\,m^{-1}\,K^{-1}$
l	helical tape length	m
L	length of the test section	m
M_h	momentum of the helical fluid	$kg\,m^{-2}\,s^{-2}$
M_T	total momentum of the axial flow	$kg\,m^{-2}\,s^{-2}$
$\dot{m}_h$	mass flow rate of the fluid through the helical channel	$kg\,s^{-1}$
$\dot{m}_T$	total mass flow rate of fluid at the test section exit	$kg\,s^{-1}$
N_h	helical channel number	
Nu_0	Nusselt number for non-swirling flow	
Nu_s	Nusselt number for swirl flow	
Nu^*	normalized Nusselt number, $Nu_s Nu_0^{-1}$	
Pr	Prandtl number, $\mu C_p k^{-1}$	
Q	heat transfer rate based on test section surface area	W
δR	uncertainty in the result	
Re	Reynolds number	
T	temperature	K
T_b	Local bulk temperature calculated from heat balance	K
T_w	wall temperature of the test section	K
ΔT	temperature difference between the wall and fluid	K
u	mean velocity	$m\,s^{-1}$
W	helical channel width	m
X_i	ith variable	

Greek symbols

α	helical angle	
η	performance efficiency	
ρ	density	$kg\,m^{-3}$
μ	dynamic viscosity	$N\,m^{-2}\,s$
ν	kinematic viscosity	$m^2\,s^{-1}$

Subscripts

a	ambient
b	bulk
h	helical tape
i	inlet
o	equivalent smooth tube value
s	swirl flow
T	total
w	wall
x	point or local

length of test section; while others are fixed at the inlet, and decay of swirl along the tube is permitted. These techniques can increase heat transfer coefficient due to related flow patterns, giving the facility of designing smaller exchanger or of upgrading existing exchangers [6,7]. In other applications, effective heat remove may be desirable to prevent excessive temperatures when a certain amount of energy is to be dissipated over a limited area. In the swirling flows pressure loss occurs so they bring additional pumping power and construction costs, and total cost of a heat exchanger increases [8,9].

Bergles [10] cited nearly 250 publications on swirl flows until of the end of 1983. Approximately 140 of these articles were related to heat transfer enhancement. F. Change and Dhir [11] successfully used tangential injection, to obtain swirl flow for the enhancement of critical heat flux. They obtained an average enhancement of 35 to 40 percent in heat transfer on a constant pumping power basis.

Another technique of enhancing heat transfer coefficient is the use of the vertical flow. A detailed description of this kind of flow and its potential in heat transfer enhancement were given by Razgaitis and Holman [12]. According to them, one promising technique for the augmentation of convective heat transfer is the use of confined swirl flow, particularly of the decaying vortex type.

Kreith and Margolis [13] suggested that swirl flow obtained by tangentially injection of some part of the fluid upon the axial channel flow can lead to an enhancement in heat transfer. But they did not carry out any experiment to support their proposal.

Although extensive research has already been done on enhancing heat transfer in tubes inserting a swirl element along the axis or at the entrance, the past effort has focused on the effects of geometrical properties of the swirling elements on heat transfer and frictional losses. In this study, flow ratio (the ratio of swirling flow to non-swirling flow) is considered on account of heat transfer enhancement and pressure drop in turbulent flow. The objective of this research is therefore to investigate the effect of momentum ratio—inserting a swirling element at the entrance of a tube—on heat transfer and pressure drop, experimentally.

2. Experimental setup

The flow loop used for this study is shown schematically in Fig. 1. The system is consisted of mainly a pump, three visual flow meters, a test section, pressure transmitters, a reservoir tank, data logger and thermocouples. The experimental set-up comprises of two parts: the swirl generator and the test section.

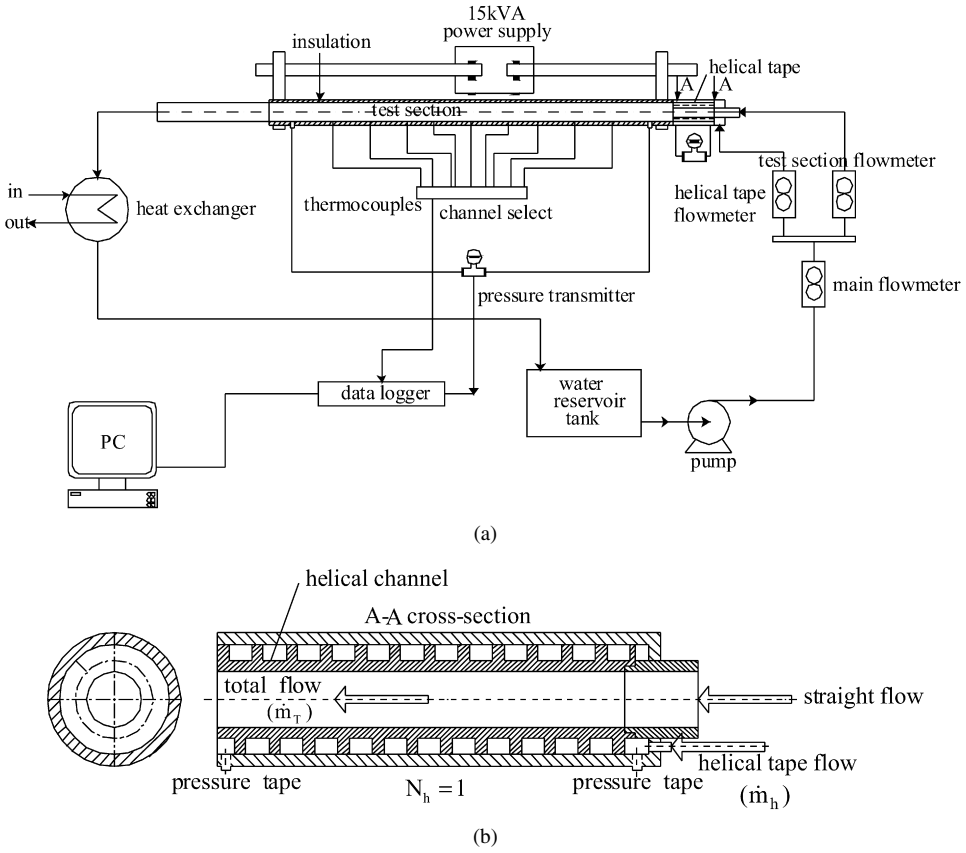

Fig. 1. (a) Schematic diagram of the flow loop; (b) Detail of the helical tape.

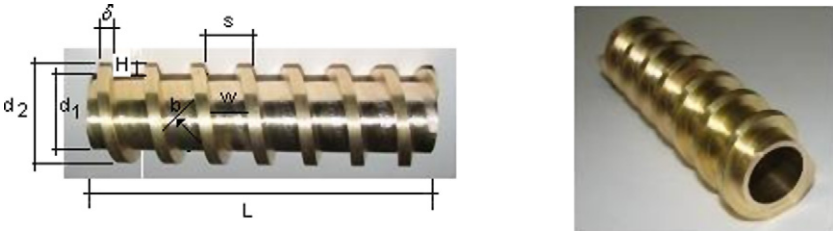

Fig. 2. Photograph of helical tape.

The test section is made of smooth stainless steel pipe with the dimensions of 1000 mm length and 20 mm inner diameter. The details of the swirl generator (helical tape) design were also shown in Figs. 1 and 2. The inner diameter and the length of the helical tape are $d_1 = 13$ mm and $l = 100$ mm, respectively. Helical channel is milled on this tape with various angles ($\alpha = 30°, 45°, 60°$) and numbers ($N_h = 1, 2$). The depth of the channel is 3.5 mm. The helical tape is tight fitted to the main pipe as shown in Fig. 1. The total flow rate is measured with a main flow meter, thereafter the flow is divided into two ways: one to the inner part of this helical tape and the other through the helical channel. Eventually, the total flow at the exit of the helical tape includes the flow through the inner and outer parts of the helical tape.

The test section was ohmically heated with current provided from a 15 kW DC power supply. Consequently, the pipe is heated uniformly and in order to prevent voltage fluctuations, a voltage regulator was employed. In order to reduce heat loss, the outer surface of the test section was insulated with glass wool. The entrance and exit temperatures of the air and the wall temperatures were measured with copper-constant thermocouples at ten axial stations, located just after the helical tape at the distances of $x/L = 0.1, 0.2, 0.3, 0.4, 0.5, 0.6, 0.7, 0.8, 0.9, 1$ from the inlet to the end of the test section. The thermocouples were isolated with a very thin sheet of mica between the thermocouple and the tube surface so as not to be effected from electricity. All temperature data from the test section were recorded via a data acquisition module. The bulk temperatures of the fluid at the inlet were measured with the two thermocouples. The local bulk temperatures of the water were calculated assuming a liner relationship between the inlet and exit bulk temperatures. This linearity results from a constant heat flux condition with negligible heat transfer along the pipe length [14,15]. Two pressure taps were located on the test pipe to measure the differential pressure drop along the length of the pipe

while the other two pressure taps were located on the helical tape.

3. Experimental uncertainty

In this study, the estimations method of Moffat [16] was used. The effect of the uncertainty in a single measurement on the calculated result, if only that one measurement were in error would be

$$\delta R_{X_i} = \frac{\partial R}{\partial X_i}\delta X_i \tag{1}$$

When several independent variables are used in the function R, the individual terms are combined by root-sum-square method.

$$\delta R = \left\{\sum_{i=1}^{N}\left(\frac{\partial R}{\partial X_i}\delta X_i\right)^2\right\}^{1/2} \tag{2}$$

Considering the relative errors in the individual factors denoted by x_n, error estimation the following equation;

$$w_{(k,h,D,f,\dot{v},\ldots)} = \left[(x_1)^2 + (x_2)^2 + \cdots + (x_n)^2\right]^{1/2} \tag{3}$$

Nusselt number uncertainties can be calculated by combinations of Eqs. (4) and (5)

$$Nu = \frac{hD}{k} \tag{4}$$

$$w_{Nu} = \left[\left(\frac{\partial Nu}{\partial h}w_h\right)^2 + \left(\frac{\partial Nu}{\partial D}w_D\right)^2 + \left(\frac{\partial Nu}{\partial k}w_k\right)^2\right]^{1/2} \tag{5}$$

$$\frac{w_{Nu}}{Nu} = \left[\left(\frac{w_h}{h}\right)^2 + \left(\frac{w_D}{D}\right)^2 + \left(\frac{w_k}{k}\right)^2\right]^{1/2} \tag{6}$$

The individual contributions to the uncertainties of the non-dimensional parameters for each of the measured physical properties are summarized in Table 1. Maximum values of uncertainty calculations for *Re*, *Nu* and f are 7.6%, 10.5% and 13.5%, respectively.

4. Heat transfer calculations

In order to determine the heat losses, the test set-up was calibrated under no-flow conditions. The calibration curve was approximated by,

$$Q_{\text{loss}} = 0.345L(\bar{T}_w - T_a) \tag{7}$$

where L, represents the length of test pipe, $\bar{T}_w$ is average wall temperature and $\bar{T}_a$ is the average ambient temperature. The average heat flux from the tube wall to the fluid is defined in terms of the nominal inside surface area,

$$Q = hA(\bar{T}_w - T_b) \tag{8}$$

It took approximately two hours to obtain a steady state for each run. Experiments were conducted for different values of heat input to check the reproducibility of the results.

Due to a small temperature gradient along the tube, the axial heat flux was essentially constant; hence it was possible to utilize the average heat flux to compute local heat transfer coefficients. The heat rate was assumed to be uniform. The thermal conductivity of test tube is a strong function of temperature. Its functional dependence on temperature was obtained from the work of Hogan [17]. The bulk temperature at each position was computed assuming a linear variation along the heated length, and heat transfer coefficient was then found from the following equation,

$$h_{x,i} = \frac{\dot{q}}{T_{w,i} - T_{b,i}} \tag{9}$$

where $(h_{x,i})$ is the local heat transfer coefficient, $\dot{q} = (Q_{\text{net}}/A)$ is the local heat transfer rate per unit from the wall to water, $(T_{w,i})$ is the local wall temperature of the tube and, $T_{b,i}$ is the local bulk mean water temperature. The inside tube wall temperature was obtained by correcting the measured outside wall temperature by solving the cylindrical heat conduction equation from measured outside wall temperature; the one dimensional steady-sated heat conduction equation with variable thermal conductivity was solved numerically. The local liquid bulk temperature was calculated from the heat balance and local Nusselt number was calculated as

$$Nu_{x,i} = \frac{h_i D_h}{k} \tag{10}$$

$$Re = \frac{uD_h}{\nu} \tag{11}$$

The local values for *Nu*, *Pr* and *Re* were calculated on the basis of water properties corresponding to the bulk fluid temperature, and the average values were obtained by numerical integration. In Eq. (11) *Re* is defined based on the total flow in the test section. In the experimental results, normalized Nusselt number is defined as follow,

$$Nu^* = \frac{Nu_s}{Nu_0} \tag{12}$$

where Nu_s is Nusselt number for swirl flow and Nu_0 is the Nusselt number for fully developed axial flow in the tube without helical tape calculated according to Eq. (10).

In this work, swirl intensity is expressed as the ratio of tangential momentum of the helical fluid to the axial momentum of the total flow and this equation expressed by Guo and Dhir [18].

$$\frac{M_h}{M_T} = \frac{\dot{m}_h^2}{\dot{m}_T^2}\frac{A}{A_h} \tag{13}$$

where $\dot{m}_h$ is the flow rate of the water through the helical channel and $\dot{m}_T$ is the total mass flow rate of the water through the

Table 1
Typical uncertainties for the relevant variable

Variable	Uncertainty (%)
Water density, ρ	1.5
Specific heat of water, C_p	3.1
Dynamic viscosity of water, μ	2.7
Hydraulic diameter, D_h	1.1
Thermal conductivity of water, k	2.3
Water flow rate, $\dot{m}$	4.5
Pressure drop, ΔP	4.3

test section. A and A_h are the cross-sectional area of the test section and total area of the helical channel, respectively.

Eq. (13), can be rearranged for helical swirl generator

$$\frac{M_h}{M_T} = \left(\frac{\dot{m}_h}{\dot{m}_T}\right)^2 \left(\frac{W.H}{\pi D^2/4}\right) \frac{\mathrm{Sin}\,\alpha}{N_h} \tag{14}$$

where N_h is the number of channel on the helical tape, W and H are the helical channel width and height, respectively. It is important to compare the experimental data obtained for Nusselt number in fully developed axial flow with the correlations from the literature. Nusselt numbers calculated from the experimental data were compared with the correlation recommended by Petukhov [19];

$$Nu_0 = \frac{(f/8)Re\,Pr}{1.07 + 12.7\sqrt{f/8}(Pr^{2/3} - 1)} \left(\frac{\mu_b}{\mu_w}\right)^{0.11} \quad (\text{for } T_w > T_b) \tag{15}$$

f, is friction factor and for smooth tubes it is given as [19];

$$f = \left(1.82\log_{10}(Re) - 1.64\right)^{-2} \tag{16}$$

So as to determine the friction factor for both test section and helical tape, pressure drop across the helical channel and across the test section are measured separately. The friction factor is then obtained by the following equation:

$$f = \frac{\Delta P}{(\frac{L}{D_h})\rho\frac{v^2}{2}} \tag{17}$$

5. Experimental results and discussion

Experimentally determined Nusselt values for smooth tube (without helical tape) are compared with Dittus–Boelter correlation [20,21], Petukov correlation [21], and Sieder and Tate correlation [21] for turbulent flow, in Fig. 3. It is seen that the experimental results of the present work are in good agreement with the aforementioned studies.

Fig. 4 shows the comparison of friction factors for the test section determined from the present experimental work and from the correlation of Eq. (16). It is seen that swirl generators cause a considerable increase in friction factor. The increment of friction factor for swirl element with $\alpha = 60°$, $N_h = 1$ and $M_h/M_T = 8.56$ is about 2.1 times in comparison with non-swirl flow. The friction factor decreases with increasing Re number and increase with increasing momentum ratio. A similar tendency can be seen in Fig. 5 in which friction across the helical channel is plotted versus Reynolds number. When compared to the friction across the smooth pipe, the friction factor is about 2.5–5 times higher than the non-swirl flow depending on the momentum ratio and Reynolds number, in Fig. 5.

Ratio of Nusselt number for swirling flow to none swirling represents the heat transfer enhancement. In Figs. 6–8 the heat transfer enhancements for different momentum ratios are plotted as a function of axial distance from the helical tape exit. The increase in heat transfer coefficient was found to be strongly depending on the momentum ratio M_h/M_T. This heat transfer augmentation is entirely due to the thinner thermal and hydrodynamic boundary layers caused by swirling flow. Increases in local velocity with swirl generator may intensify the flow

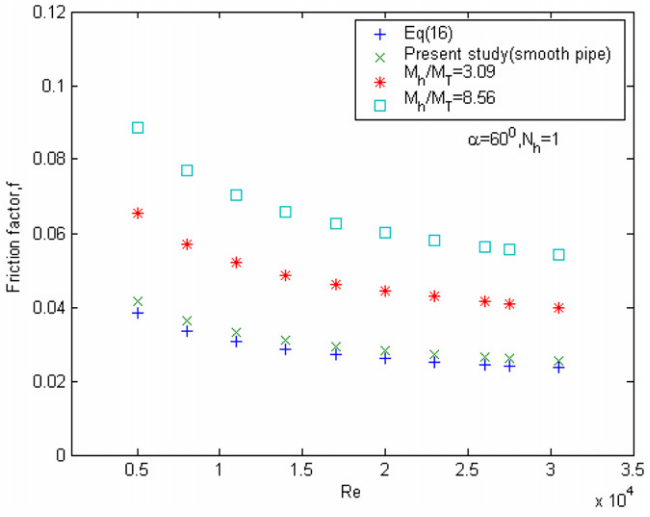

Fig. 4. Friction coefficient variations for the test section with respect to Re.

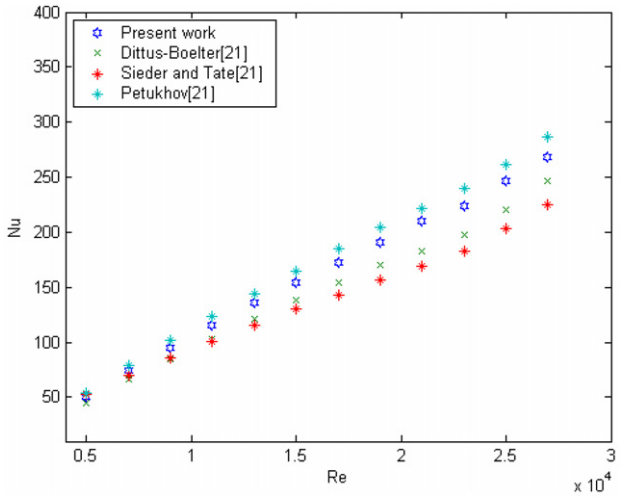

Fig. 3. Data verification of average Nusselt number for the smooth tube.

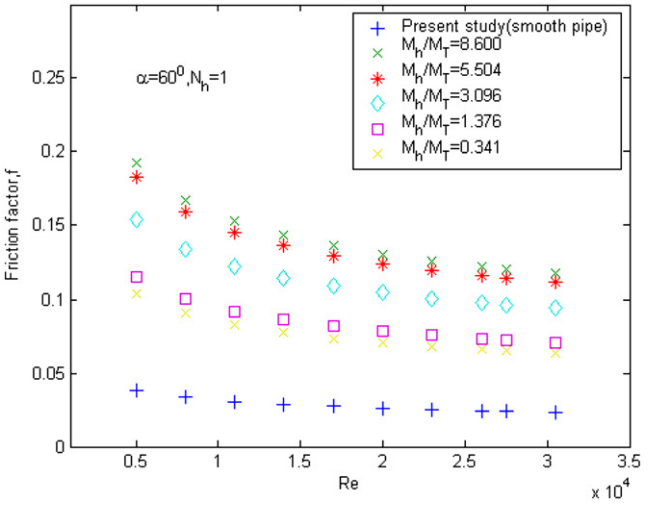

Fig. 5. Friction coefficient variations for the helical channel with respect to Re.

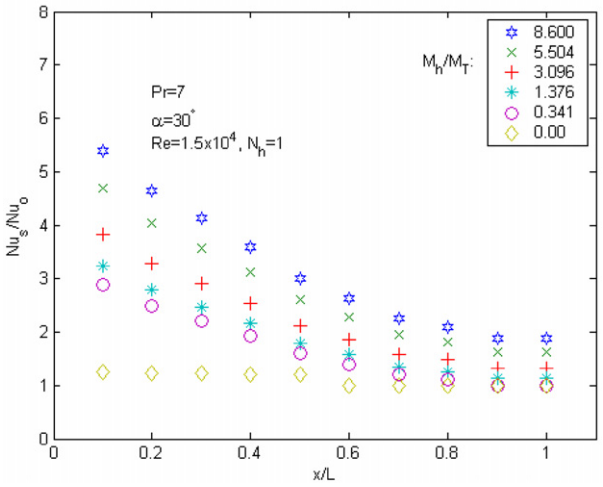

Fig. 6. Normalized Nusselt number distribution along test section for different momentum ratios.

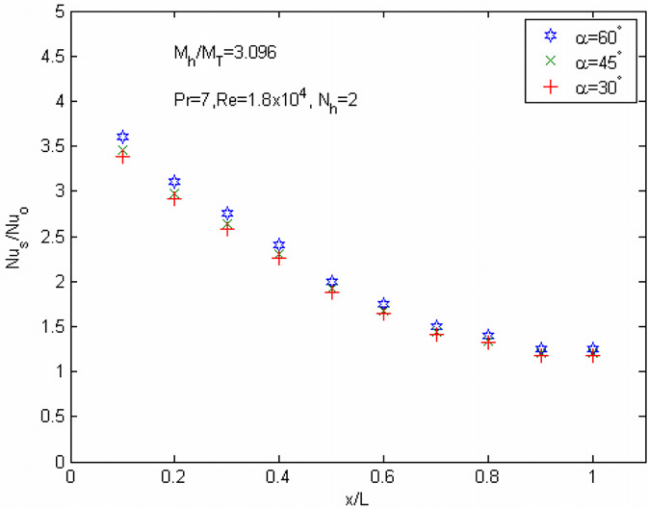

Fig. 8. The effect of helical angle on normalized Nusselt number.

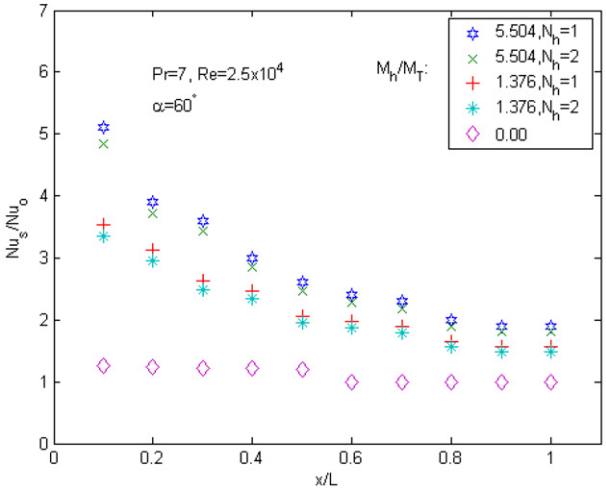

Fig. 7. Effect of the helical channel number on normalized Nusselt.

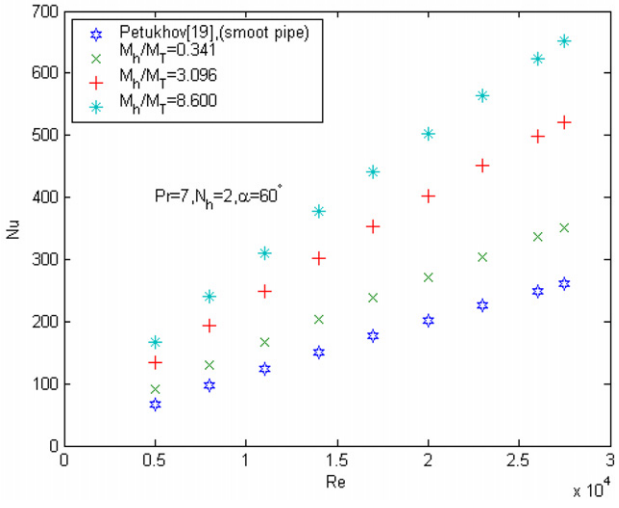

Fig. 9. Variation of average Nusselt number with *Re* for different momentum ratios.

turbulence. It can be seen that local heat transfer coefficient decreases along the tube axis because tangentially momentum decreases due to the viscous dissipation and fluid mixing.

So as to illustrate the effect of helical channel number on heat enhancement, normalized local Nusselt number is plotted as a function of axial distance for a constant Prandtl number and for one helical channel ($N_h = 1$) and two helical channels ($N_h = 2$) with 60° angle in Fig. 7. But it is seen from this figure that the main trend for both one and two channels seems to be nearly the same. The enhancement is only a little higher with one helical channel for both momentum ratios. Helical channel number has no significant effect on Nu_s/Nu_0. It is clear, however, that the increase in heat transfer coefficient at a given location is found to be strongly depended on the momentum ratio M_h/M_T. The magnitude of the heat transfer in swirl flow is much larger than the one observed in the thermally developing region of purely axial flow.

The local Nusselt number decrease along the test section with the increasing axial distance, but at much smaller decreasing rate than for the flow of the smooth tube without a helical tape. This decrease is more pronounced at higher momentum ratios.

In order to analyze the effect of the helical angle on heat transfer, normalized *Nu* number is plotted versus x/L for three different helical angles, in Fig. 8. This figure demonstrates that heat transfer enhancement is weakly affected by the helical angle.

Average Nusselt number versus Reynolds number is plotted in Fig. 9. As mentioned above for local *Nu* numbers, increasing momentum ratio causes an increase also in average Nusselt number.

6. Performance criteria

It is necessary to determine the efficiency of this experimental set-up with and without a swirl flow under the condition of constant pumping power. The heat transfer enhancement efficiency for constant pumping power can be expressed as follows [22,23]:

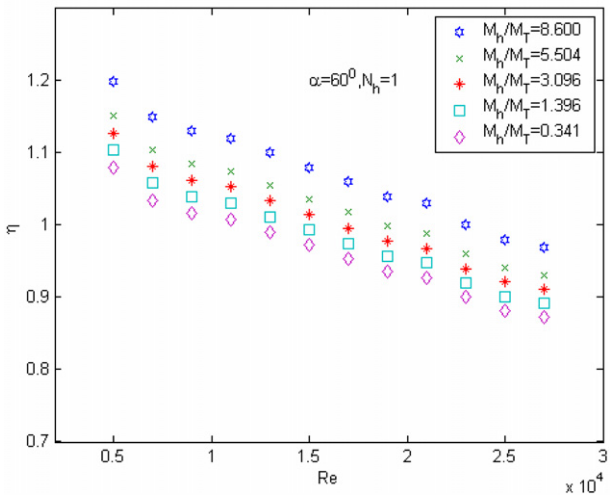

Fig. 10. Variation of heat enhancement efficiency with Reynolds number.

$$\eta = \left(\frac{h_s}{h_0}\right)_p \tag{18}$$

The heat transfer efficiency versus Reynolds number for various momentum ratios is plotted in Fig. 10. It is seen that the heat transfer efficiency increases with the increasing momentum ratio while decreases with increasing Reynolds number. Enhancement efficiencies varied between 0.97–1.20 for the highest momentum ratio of $M_h/M_T = 8.600$ and, 0.873–1.08 for the lowest momentum ratio of $M_h/M_T = 0.341$, depending on Reynolds number. It is obvious that, for a net energy gain the value of η must be greater than unity. As can be seen in Fig. 10, η is higher than unity for $M_h/M_T = 8.600$ and $Re > 22\,000$. However, for the lowest momentum ratio $M_h/M_T = 0.341$, η is higher than unity only if Re is bigger than 10 000. Consequently, the helical tape will cause an energy loss rather than gain below the mentioned Re values at which η is lower than unity.

7. Conclusions

(1) For the range of experimental conditions, the swirl flow heat transfer coefficients were found to be higher than fully developed non-swirling flow.
(2) The highest local heat transfer coefficient was obtained at the highest momentum ratio. However, the enhancement in the heat transfer decays along the tube due to the decay in swirl flow.
(3) An enhancement up to 300% in local heat transfer coefficient was observed in the swirl flow compared to the fully developed axial flow for the same fluid velocity depending on momentum ratio and Re.
(4) Helical channel number and helical angle has no significant effect on Nu_s/Nu_0. The enhancement is a little higher with one helical channel and with helical angle of $\alpha = 60°$.
(5) For the highest momentum ratio a net energy gain up to 20% was achieved depending on Re number.

References

[1] E. Smithberg, F. Landis, Friction and forced convection heat transfer characteristics in tubes fitted with twisted tape swirl generators, ASME J. Heat Transfer 2 (1964) 39–49.
[2] A.W. Date, J.R. Singham, Numerical prediction of friction factor and heat transfer characteristics of fully developed laminar flow in tubes containing twisted tapes, ASME 94 (9) (1972) 54–58.
[3] A.W. Date, Prediction of fully developed flow in tube containing a twisted tape, Int. J. Heat Mass Transfer 17 (1974) 845–859.
[4] S.W. Hong, A.E. Bergles, Augmentation of laminar flow heat transfer in tubes by means of twisted-tape inserts, ASME J. Heat Transfer 98 (2) (1976) 251–256.
[5] S. Eiamsa-ard, P. Promvonge, Enhancement of heat transfer in a tube with regularly spaced helical tape swirl generators, Solar Energy 78 (2005) 483–494.
[6] W.J. Marner, A.E., Bergles, in: 6th Int. Heat Transfer Conf., Toronto, Canada, vol. 2, 1978, pp. 583.
[7] A.H. Algifri, R.K. Bahardwaj, Y.V.N. Rao, Heat transfer in turbulent decaying swirl flow in a circular pipe, Int. J. Heat Transfer 31 (8) (1988) 1563–1568.
[8] A. Durmuş, Heat exchanger and exergy loss in concentric heat exchanger with snail entrance, Int. Commun. Heat Mass Transfer 29 (3) (2002) 303–312.
[9] M. Yılmaz, O. Comakli, S. Yapici, O.N. Sara, Heat transfer and fraction characteristics in decaying swirl flow generated by different radial guide vane swirl generators, Energy Convers. Manag. 44 (2003) 283–300.
[10] E. Bergles, Heat transfer enhancement—the encouragement and accommodation of high heat fluxes, J. Heat Transfer Trans. ASME 119 (1997) 8–19.
[11] F. Change, V.K. Dhir, Turbulent flow field in tangentially injected swirl flow in tubes, Int. J. Heat Fluid Flow 15 (1994) 346–356.
[12] R. Razgaitis, J.P. Holman, Survey of heat transfer in confined swirl flow, Heat Mass Trans. Process. 2 (1976) 831–866.
[13] F. Kreith, D. Margolis, Heat transfer and friction in turbulence vortex flow, Appl. Sci. Res. 8 (1959) 457–473.
[14] H. Algifri, R.K. Bhardwaj, Y.V.N. Rao, Heat transfer in turbulent decaying swirl flow in a circular pipe, Int. J. Heat Mass Transfer 31 (8) (1988) 1563–1568.
[15] O. Kitoh, Axi-asymmetric character of turbulent swirling flow in a straight circular pipe, Bull. JSME 27 (226) (1984) 683–690.
[16] R.J. Moffat, Describing the uncertainties in experimental results, Experimental Thermal Fluid Sci. 1 (1988) 3–17.
[17] C.L. Hogan, The thermal conductivity of metals at high temperature, PhD dissertation Lehigh University, 1950.
[18] Z. Guo, V.K. Dhir, Single- and two-phase heat transfer in tangential injection-induced swirl flow, Int. J. Heat Fluid Flow 10 (3) (1989) 203–210.
[19] B.S. Petukhov, Heat transfer and fraction in turbulent pipe flow with variable physical properties, in: Advances in Heat Transfer, vol. 6, Academic Press, San Diego, 1970, pp. 504–564.
[20] Y.A. Cengel, Heat Transfer: A Practical Approach, second ed., McGraw-Hill, New York, 1998.
[21] F.P. Incropera, D.P. De Witt, Introduction to Heat Transfer, John Wiley and Sons, New York, 1990, pp. 456–457.
[22] S. Eiamsa-ard, P. Promvonge, Experimental investigation of heat transfer and friction characteristics in a circular tube fitted with V-nozzle turbulators, Int. Commun. Heat Mass Transfer 33 (2006) 591–600.
[23] K. Bilen, U. Akyol, S. Yapıcı, Heat transfer and friction correlations and thermal performance analysis for a finned surface, Energy Convers. Manag. 42 (2001) 1071–1083.